7 Photon-Axion Conversion in Intergalactic Magnetic Fields and Cosmological Consequences

Alessandro Mirizzi,[1] Georg G. Raffelt[1] and Pasquale D. Serpico[2]

[1] Max-Planck-Institut für Physik (Werner-Heisenberg-Institut)
Föhringer Ring 6, 80805 München, Germany
raffelt@mppmu.mpg.de
[2] Center for Particle Astrophysics, Fermi National Accelerator Laboratory
Batavia, IL 60510-0500, USA
serpico@fnal.gov

Abstract. Photon-axion conversion induced by intergalactic magnetic fields causes an apparent dimming of distant sources, notably of cosmic distance indicators such as supernovae of type Ia (SNe Ia). We review the impact of this mechanism on the luminosity-redshift relation of SNe Ia, on the dispersion of quasar spectra, and on the spectrum of the cosmic microwave background. The original idea of explaining the apparent dimming of distant SNe Ia without cosmic acceleration is strongly constrained by these arguments. However, the cosmic equation of state extracted from the SN Ia luminosity-redshift relation remains sensitive to this mechanism. For example, it can mimic phantom energy.

7.1 Introduction

The two-photon coupling of axions or axion-like particles allows for transitions between them and photons in external electric or magnetic fields as shown in Fig. 7.1 [1, 2]. This mechanism serves as the basis for the experimental searches for galactic dark matter axions [1, 3] and solar axions [1, 4, 5, 6, 7]. The astrophysical implications of this mechanism have also been widely investigated and reviewed [8, 9]. The phenomenological consequences of an extremely light or massless axion would be particularly interesting in several astrophysical circumstances such as polarization of radio-galaxies [10] and quasars [11], the diffuse X-ray background [12], or ultra-high energy cosmic rays [13, 14].

One intriguing cosmological consequence of this mechanism is photon-axion conversion caused by intergalactic magnetic fields, leading to the dimming of distant light sources, notably of supernovae (SNe) of type Ia that are used as cosmic distance indicators [15]. Observationally, SNe Ia at redshifts, $0.3 \lesssim z \lesssim 1.7$, appear fainter than expected from the luminosity-redshift relation in a decelerating Universe [16, 17, 18], a finding usually interpreted as evidence for acceleration of the cosmic expansion rate and thus for a cosmic equation of state (EoS) that today is dominated by a cosmological constant,

A. Mirizzi et al.: *Photon-Axion Conversion in Intergalactic Magnetic Fields and Cosmological Consequences*, Lect. Notes Phys. **741**, 115–134 (2008)
DOI 10.1007/978-3-540-73518-2_7

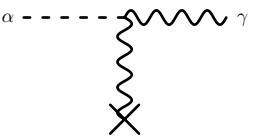

Fig. 7.1. Axion-photon transition in an external electric or magnetic field

a slowly evolving scalar field, or something yet more exotic [19]. The dimming caused by photon-axion conversion could mimic this behavior and thus provide an alternative to the interpretation as cosmic acceleration. Although still requiring some non-standard fluid to fit the flatness of the Universe, this model seemed capable of explaining the SN-dimming through a completely different mechanism.

However, if the light from distant SNe Ia reaches us partially converted to axion-like particles, the same mechanism would affect all distant sources of electromagnetic radiation. Therefore, it appears useful to update the different arguments constraining photon-axion conversion in intergalactic magnetic fields, in particular the constraints arising from spectral distortions of the cosmic microwave background (CMB) and dispersion of quasar (QSO) spectra.

To this end, we begin in Sect. 7.2 with a review of the formalism of photon-axion conversion in magnetic fields. Some technical details are deferred to Appendix A. In Sect. 7.3 we describe how this mechanism affects the SN Ia luminosity-redshift relation and accounts for the observed dimming. In Sect. 7.4 we turn to spectral CMB distortions and in Sect. 7.5 combine these limits with those from the dispersion of QSO spectra. In Sect. 7.6 we describe some additional limits from a violation of the reciprocity relation between the luminosity and angular diameter distances. We conclude in Sect. 7.7 with comments on the viability of the photon-axion conversion mechanism.

7.2 Photon-Axion Conversion

To understand how photon-axion conversion could affect distant sources, we take a closer look at the phenomenon of photon-axion mixing. The Lagrangian (density) describing the photon-axion system is [8]

$$L = L_\gamma + L_a + L_{a\gamma\gamma} \, . \tag{7.1}$$

The QED Lagrangian for photons is

$$L_\gamma = -\frac{1}{4} F_{\mu\nu} F^{\mu\nu} + \frac{\alpha^2}{90 m_e^4} \left[(F_{\mu\nu} F^{\mu\nu})^2 + \frac{7}{4} (F_{\mu\nu} \tilde{F}^{\mu\nu})^2 \right] \, , \tag{7.2}$$

where $F_{\mu\nu}$ is the electromagnetic field-strength tensor, $\tilde{F}_{\mu\nu} = \frac{1}{2} \varepsilon_{\mu\nu\varrho\sigma} F^{\varrho\sigma}$ its dual, α the fine-structure constant, and m_e the electron mass. We always

use natural units with $\hbar = c = k_{\rm B} = 1$. The second term on the RHS is the Euler-Heisenberg effective Lagrangian, describing the one-loop corrections to classical electrodynamics for photon frequencies $\omega \ll m_e$. The Lagrangian for the non-interacting axion field a is

$$L_a = \frac{1}{2}\partial^\mu a\, \partial_\mu a - \frac{1}{2}m^2 a^2 \ . \tag{7.3}$$

A generic feature of axion models is the CP-conserving two-photon coupling, so that the axion-photon interaction is

$$L_{a\gamma\gamma} = -\frac{1}{4}\, g_{a\gamma\gamma} F_{\mu\nu}\tilde{F}^{\mu\nu} a = g_{a\gamma\gamma}\, \mathbf{E}\cdot\mathbf{B}\, a \ , \tag{7.4}$$

where $g_{a\gamma\gamma}$ is the axion-photon coupling with dimension of inverse energy. A crucial consequence of L is that the propagation eigenstates of the photon-axion system differ from the corresponding interaction eigenstates. Hence, interconversion takes place, much in the same way as for massive neutrinos of different flavors. However, as the mixing term $F_{\mu\nu}\tilde{F}^{\mu\nu}a$ involves two photons, one of them must correspond to an external field [1, 2, 8, 20].

Axion-photon oscillations are described by the coupled Klein-Gordon and Maxwell equations implied by these Lagrangians. For very relativistic axions ($m_a \ll \omega$), the short-wavelength approximation can be applied, and the equations of motion reduce to a first-order propagation equation. More specifically, we consider a monochromatic light beam traveling along the z-direction in the presence of an arbitrary magnetic field $\mathbf{B}$. Accordingly, the propagation equation takes the form [2]

$$(\omega - {\rm i}\partial_z + \mathcal{M}) \begin{pmatrix} A_x \\ A_y \\ a \end{pmatrix} = 0 \ , \tag{7.5}$$

where A_x and A_y correspond to the two linear photon polarization states, and ω is the photon or axion energy. The mixing matrix is

$$\mathcal{M} = \begin{pmatrix} \Delta_{xx} & \Delta_{xy} & g_{a\gamma\gamma}B_x/2 \\ \Delta_{yx} & \Delta_{yy} & g_{a\gamma\gamma}B_y/2 \\ g_{a\gamma\gamma}B_x/2 & g_{a\gamma\gamma}B_y/2 & \Delta_a \end{pmatrix} \ , \tag{7.6}$$

where $\Delta_a = -m_a^2/2\omega$. The component of $\mathbf{B}$ parallel to the direction of motion does not induce photon-axion mixing. The terms proportional to B have an evident physical meaning, but the Δ_{ij}-terms ($i, j = x, y$) require some explanation. Generally speaking, they are determined both by the properties of the medium and by the QED vacuum polarization effect. We ignore the latter, being sub-dominant for the problem at hand [21].

For a homogeneous magnetic field, we may choose the y-axis along the projection of $\mathbf{B}$ perpendicular to the z-axis. Correspondingly we have $B_x = 0$, $B_y = |\mathbf{B}_{\rm T}| = B\sin\theta$, $A_x = A_\perp$, and $A_y = A_\parallel$. Equation (7.5) then becomes

$$(\omega - \mathrm{i}\partial_z + \mathcal{M}) \begin{pmatrix} A_\perp \\ A_\parallel \\ a \end{pmatrix} = 0 \,, \tag{7.7}$$

with the mixing matrix

$$\mathcal{M} = \begin{pmatrix} \Delta_\perp & \Delta_{\mathrm{R}} & 0 \\ \Delta_R & \Delta_\parallel & \Delta_{a\gamma} \\ 0 & \Delta_{a\gamma} & \Delta_a \end{pmatrix} \,, \tag{7.8}$$

where

$$\Delta_{a\gamma} = \frac{g_{a\gamma\gamma}}{2} |\mathbf{B}_{\mathrm{T}}| \,, \tag{7.9}$$

$$\Delta_{\parallel,\perp} = \Delta_{\mathrm{pl}} + \Delta^{\mathrm{CM}}_{\parallel,\perp} \,. \tag{7.10}$$

In a plasma, the photons acquire an effective mass given by the plasma frequency $\omega^2_{\mathrm{pl}} = 4\pi\alpha\, n_e/m_e$, with n_e the electron density, leading to

$$\Delta_{\mathrm{pl}} = -\frac{\omega^2_{\mathrm{pl}}}{2\omega} \,. \tag{7.11}$$

Furthermore, the $\Delta^{\mathrm{CM}}_{\parallel,\perp}$ terms describe the Cotton-Mouton effect, i.e., the birefringence of fluids in the presence of a transverse magnetic field where $|\Delta^{\mathrm{CM}}_\parallel - \Delta^{\mathrm{CM}}_\perp| \propto B^2_{\mathrm{T}}$. These terms are of little importance for the following arguments and will thus be neglected. Finally, the Faraday rotation term Δ_{R}, which depends on the energy and the longitudinal component B_z, couples the modes $A_\parallel$ and $A_\perp$. While Faraday rotation is important when analyzing polarized sources of photons, it plays no role in the problem at hand.

With this simplification the $A_\perp$ component decouples, and the propagation equations reduce to a 2-dimensional mixing problem with a purely transverse field $\mathbf{B} = \mathbf{B}_{\mathrm{T}}$

$$(\omega - \mathrm{i}\partial_z + \mathcal{M}_2) \begin{pmatrix} A_\parallel \\ a \end{pmatrix} = 0 \,, \tag{7.12}$$

with a 2-dimensional mixing matrix

$$\mathcal{M}_2 = \begin{pmatrix} \Delta_{\mathrm{pl}} & \Delta_{a\gamma} \\ \Delta_{a\gamma} & \Delta_a \end{pmatrix} \,. \tag{7.13}$$

The solution follows from diagonalization by the rotation angle

$$\vartheta = \frac{1}{2} \arctan\left(\frac{2\Delta_{a\gamma}}{\Delta_{\mathrm{pl}} - \Delta_a} \right) \,. \tag{7.14}$$

In analogy to the neutrino case [22], the probability for a photon emitted in the state $A_\parallel$ to convert into an axion after travelling a distance s is

$$P_0(\gamma \to a) = \left|\langle A_\parallel(0)|a(s)\rangle\right|^2 = \sin^2(2\vartheta)\sin^2(\Delta_{\rm osc}s/2)$$
$$= (\Delta_{a\gamma}s)^2\,\frac{\sin^2(\Delta_{\rm osc}s/2)}{(\Delta_{\rm osc}s/2)^2}\,, \qquad (7.15)$$

where the oscillation wavenumber is given by

$$\Delta_{\rm osc}^2 = (\Delta_{\rm pl} - \Delta_a)^2 + 4\Delta_{a\gamma}^2\,. \qquad (7.16)$$

The conversion probability is energy-independent when $2|\Delta_{a\gamma}| \gg |\Delta_{\rm pl} - \Delta_a|$ or whenever the oscillatory term in (7.15) is small, i.e., $\Delta_{\rm osc}s/2 \ll 1$, implying the limiting behavior $P_0 = (\Delta_{a\gamma}s)^2$.

The propagation over many B-field domains is a truly 3-dimensional problem because different photon polarization states play the role of $A_\parallel$ and $A_\perp$ in different domains. This average is enough to guarantee that the conversion probability over many domains is an incoherent average over magnetic field configurations and photon polarization states. The probability after traveling over a distance $r \gg s$, where s is the domain size, is derived in Appendix A along the lines of [23] and is found to be

$$P_{\gamma\to a}(r) = \frac{1}{3}\left[1 - \exp\left(-\frac{3P_0\,r}{2s}\right)\right]\,, \qquad (7.17)$$

with P_0 given by (7.15). As expected, for $r/s \to \infty$ the conversion probability saturates, so that on average one third of all photons converts to axions.

7.3 Photon-Axion Conversion and Supernova Dimming

7.3.1 Observations

In 1998, two groups using SNe Ia as cosmic distance indicators reported first evidence for a luminosity-redshift relation that indicated that the expansion of the universe was accelerating at that time [16, 17]. The quantity relevant for SN Ia observations is the luminosity distance d_L at redshift z, defined by

$$\mathrm{d}_L^2(z) = \frac{\mathcal{L}}{4\pi\mathcal{F}}\,, \qquad (7.18)$$

where $\mathcal{L}$ is the absolute luminosity of the source and $\mathcal{F}$ is the energy flux arriving at Earth [16, 17]. In Friedmann-Robertson-Walker cosmologies, the luminosity distance at a given redshift z is a function of the Hubble parameter H_0, the matter density $\Omega_{\rm M}$, and the dark energy density Ω_Λ. Usually the data are expressed in terms of magnitudes

$$m = M + 5\log_{10}\left(\frac{d_L}{\rm Mpc}\right) + 25\,, \qquad (7.19)$$

where M is the absolute magnitude, equal to the value that m would have at $\mathrm{d}_L = 10\,\mathrm{pc}$.

Figure 7.2 shows the Hubble diagram for SN Ia samples at low and high z. The distances of high-redshift SNe are, on average, 10–15% larger than those in a low matter density ($\Omega_\mathrm{M} = 0.2$) Universe without dark energy ($\Omega_\Lambda = 0$). Therefore, objects of a fixed intrinsic brightness appear fainter, if the cosmic energy density budget is dominated by dark energy. The best fit of these data supports a Universe composed of a fraction of dark matter $\Omega_\mathrm{M} \simeq 0.3$ and a fraction of dark energy $\Omega_\Lambda \simeq 0.7$.

Dark energy has been associated with vacuum energy or an Einstein cosmological constant resulting in a constant energy density at all times. Defining the equation of state

$$w = \frac{p}{\varrho}\,, \tag{7.20}$$

the cosmological constant is characterized by $p = -\varrho$, i.e., $w = -1$. From the Friedmann equations, any component of the density budget with equation of state $w < -1/3$ causes cosmic acceleration. SN Ia data imply that $w \gtrsim -0.5$ are disfavored, supporting the cosmic acceleration of the Universe [17].

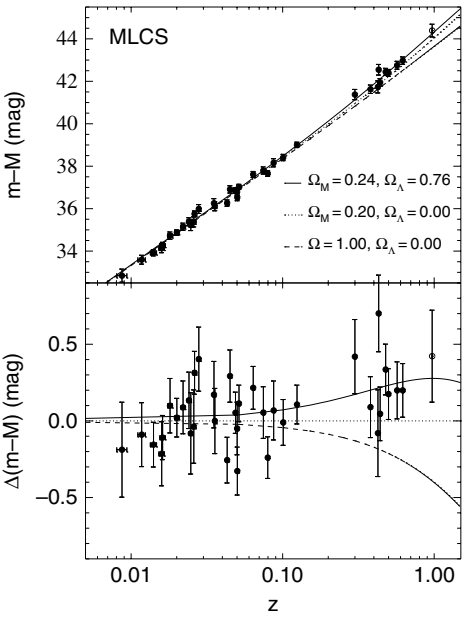

Fig. 7.2. SN Ia Hubble diagram. *Upper panel:* Hubble diagram for low- and high-redshift SN Ia samples. Overplotted are three cosmologies: "low" and "high" Ω_M with $\Omega_\Lambda = 0$ and the best fit for a flat cosmology, $\Omega_\mathrm{M} = 0.24$ and $\Omega_\Lambda = 0.76$. *Lower panel:* Difference between data and models with $\Omega_\mathrm{M} = 0.20$ and $\Omega_\Lambda = 0$ (Figure from [16] with permission)

7.3.2 Interpretation in Terms of Photon-Axion Conversion

To explore the effect of photon-axion conversion on SN-dimming, we recast the relevant physical quantities in terms of natural parameters. The energy of optical photons is a few eV. The strength of widespread, all-pervading B-fields in the intergalactic medium must be less than a few $10^{-9}\,\mathrm{G}$ over coherence lengths s crudely at the Mpc scale, according to the constraint from the Faraday effect of distant radio sources [24]. Along a given line of sight, the number of such domains in our Hubble radius is about $N \approx H_0^{-1}/s \approx 4\times10^3$ for $s \sim 1\,\mathrm{Mpc}$. The mean diffuse intergalactic plasma density is bounded by $n_e \lesssim 2.7\times10^{-7}\,\mathrm{cm}^{-3}$, corresponding to the recent WMAP measurement of the baryon density [25]. Recent results from the CAST experiment [7] give a direct experimental bound on the axion-photon coupling of $g_{a\gamma\gamma} \lesssim 1.16\times10^{-10}\,\mathrm{GeV}^{-1}$, comparable to the long-standing globular-cluster limit [8]. Suitable representations of the mixing parameters are

$$\begin{aligned}
\frac{\Delta_{a\gamma}}{\mathrm{Mpc}^{-1}} &= 0.15\; g_{10}\; B_{\mathrm{nG}}\,,\\
\frac{\Delta_{a}}{\mathrm{Mpc}^{-1}} &= -7.7\times10^{28}\left(\frac{m_a}{1\,\mathrm{eV}}\right)^2\left(\frac{\omega}{1\,\mathrm{eV}}\right)^{-1}\,,\\
\frac{\Delta_{\mathrm{pl}}}{\mathrm{Mpc}^{-1}} &= -11.1\left(\frac{\omega}{1\,\mathrm{eV}}\right)^{-1}\left(\frac{n_e}{10^{-7}\,\mathrm{cm}^{-3}}\right)\,,
\end{aligned} \tag{7.21}$$

where we have introduced $g_{10} = g_{a\gamma\gamma}/10^{-10}\,\mathrm{GeV}^{-1}$ and B_{nG} is the magnetic field strength in nano-Gauss.

The mixing angle defined in (7.14) is too small to yield a significant conversion effect for the allowed range of axion masses because $|\Delta_a| \gg |\Delta_{a\gamma}|$, $|\Delta_{\mathrm{pl}}|$. Therefore, to ensure a sufficiently large mixing angle one has to require nearly massless pseudoscalars, sometimes referred to as "arions" [26, 27]. For such ultra-light axions, a stringent limit from the absence of γ-rays from SN 1987A gives $g_{a\gamma\gamma} \lesssim 1\times10^{-11}\,\mathrm{GeV}^{-1}$ [28] or even $g_{a\gamma\gamma} \lesssim 3\times10^{-12}\,\mathrm{GeV}^{-1}$ [29]. Henceforth we will consider the pseudoscalars to be effectively massless so that our remaining independent parameters are $g_{10}B_{\mathrm{nG}}$ and n_e. Note that m_a only enters the equations via the term $m_a^2 - \omega_{\mathrm{pl}}^2$ so that for tiny but non-vanishing values of m_a, the electron density should be interpreted as $n_{e,\mathrm{eff}} = |n_e - m_a^2 m_e/(4\pi\alpha)|$.

Allowing for the possibility of photon-axion oscillations in intergalactic magnetic fields, the number of photons emitted by the source and thus the flux $\mathcal{F}$ is reduced to the fraction $P_{\gamma\to\gamma} = 1 - P_{\gamma\to a}$. Therefore, the luminosity distance (7.18) becomes

$$\mathrm{d}_L \to \mathrm{d}_L/P_{\gamma\to\gamma}^{1/2}\,, \tag{7.22}$$

and the brightness (7.19)

$$m \to m - \frac{5}{2}\log_{10}(P_{\gamma\to\gamma})\,. \tag{7.23}$$

Distant SNe Ia would eventually saturate ($P_{\gamma\to\gamma} = 2/3$) and hence, would appear $(3/2)^{1/2}$ times farther away than they really are. This corresponds to a maximum dimming of approximately 0.4 mag. Csáki, Kaloper and Terning (CKT I) showed that if photon-axion conversion takes place, this mechanism can reproduce the SN Hubble diagram [15], assuming, for example, a non-standard dark energy component $\Omega_S = 0.7$ with equation of state $w = -1/3$, which does not produce cosmic acceleration (Fig. 7.3).

However, in the model of CKT I, plasma density effects were neglected ($n_e = 0$). Later, it was recognized that the conclusions of CKT I can be significantly modified when the effects of the intergalactic plasma on the photon-axion oscillations are taken into account [21]. In the presence of plasma effects, the probability of oscillation is lower than before and it is no longer achromatic (Fig. 7.4). SN observations require not only dimming, but also that the dimming be achromatic. In fact, SN observations put a constraint on the color excess between the B and V bands,

$$E[B-V] \equiv -2.5\,\log_{10}\left[\frac{F^{\rm o}(B)}{F^{\rm e}(B)}\,\frac{F^{\rm e}(V)}{F^{\rm o}(V)}\right]\,, \tag{7.24}$$

where $F^{\rm o}$ and $F^{\rm e}$ are the observed and emitted flux, respectively. The B and V bands correspond to 0.44 μm and 0.55 μm, respectively. Observations constrain $E[B-V]$ to be lower than 0.03 [17]. This can be translated to

$$P(\gamma\to a)_V\left[\frac{P(\gamma\to a)_B}{P(\gamma\to a)_V} - 1\right] < 0.03\,. \tag{7.25}$$

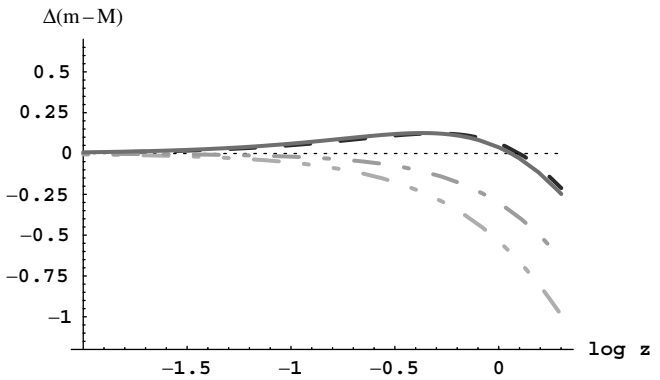

Fig. 7.3. Hubble diagram for SNe Ia for different cosmological models, relative to the curve with $\Omega_{\rm tot} = 0$ (*dotted horizontal line*). The dashed curve is a best fit to the SN data assuming that the Universe is accelerating ($\Omega_{\rm M} = 0.3$, $\Omega_\Lambda = 0.7$); the solid line is the photon-axion oscillation model with $\Omega_{\rm M} = 0.3$ and $\Omega_S = 0.7$, the dot-dashed line is $\Omega_{\rm M} = 0.3$, $\Omega_S = 0.7$ with no oscillation, the dot-dot-dashed line is for $\Omega_{\rm M} = 1$ and again no oscillation (Figure from [15] with permission)

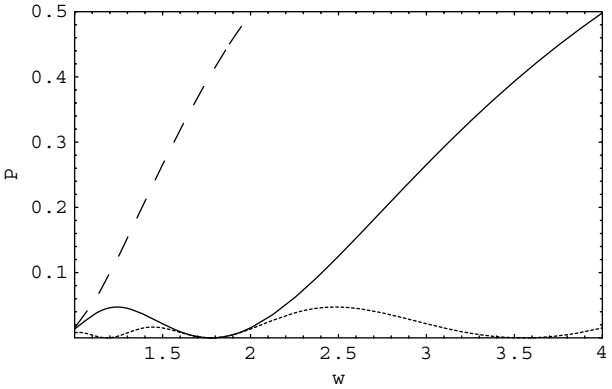

Fig. 7.4. Ratio of the probability of conversion of photons to axions including the effects of the intergalactic plasma ($n_e \approx 10^{-7}\,\mathrm{cm}^{-3}$) and the probability of oscillations when this effect is not considered, as a function of the photon energy ω. The curves are drawn for different size s of the magnetic domains: 0.5 Mpc (*dashed line*), 1 Mpc (*solid line*) and 2 Mpc (dotted line, Figure from [21] with permission)

Therefore, assuming an electron density $n_e \approx n_{\mathrm{baryons}} = n_\gamma \eta \sim 10^{-7}\,\mathrm{cm}^{-3}$, the model is ruled out in most of the parameter space because of either an excessive photon conversion or a chromaticity of the dimming [21]. Only fine-tuned parameters for the statistical properties of the extragalactic magnetic fields would still allow this explanation.

On the other hand, Csáki, Kaloper and Terning [30] (CKT II) criticized the assumed value of n_e as being far too large for most of the intergalactic space, invoking observational hints for a value at least one order of magnitude smaller. As a consequence, for $\omega_{\mathrm{pl}} \lesssim 6 \times 10^{-15}\,\mathrm{eV}$, corresponding to $n_e \lesssim 2.5 \times 10^{-8}\,\mathrm{cm}^{-3}$, one finds $|P_V - P_B| < 0.03$ so that the chromaticity effect disappears very rapidly and becomes undetectable by present observations.

Figure 7.5 shows qualitatively the regions of n_e and $g_{10} B_{\mathrm{nG}}$ relevant for SN dimming at cosmological distances. To this end, we show iso-dimming contours obtained from (7.23) for a photon energy 4.0 eV and a magnetic domain size $s = 1\,\mathrm{Mpc}$. For simplicity, we neglect the redshift evolution of the intergalactic magnetic field B, domain size s, plasma density n_e, and photon frequency ω. Our iso-dimming curves are intended to illustrate the regions where the photon-axion conversion could be relevant. In reality, the dimming should be a more complicated function since the intergalactic medium is expected to be very irregular: there could be voids of low n_e density, but there will also be high-density clumps, sheets, and filaments and these will typically have higher B fields as well. However, the simplifications used here

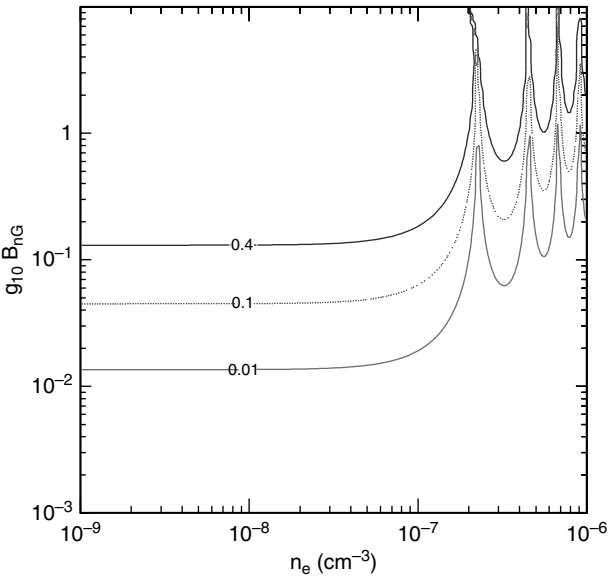

Fig. 7.5. Iso-dimming curves for an attenuation of 0.01, 0.1, and 0.4 magnitudes. The photon energy of 4.0 eV is representative of the B-band. The size of a magnetic domain is $s = 1\,\mathrm{Mpc}$ (Figure from [32] with permission)

are consistent with the ones adopted in CKT II and do not alter our main results.

The iso-dimming contours are horizontal in the low-n_e and low-$g_{10}B_{\rm nG}$ region. They are horizontal for any $g_{10}B_{\rm nG}$ when n_e is sufficiently low. From the discussion in Sect. 7.2, we know that the single-domain probability P_0 of (7.15) is indeed energy-independent when $|\Delta_{\rm osc}s| \ll 1$, i.e., for $|\Delta_{\rm pl}|s/2 \ll 1$ and $|\Delta_{a\gamma}|s \ll 1$. When $n_e \lesssim$ few $10^{-8}\,\mathrm{cm}^{-3}$ and $g_{10}B_{\rm nG} \lesssim 4$, we do not expect an oscillatory behavior of the probability. This feature is nicely reproduced by our iso-dimming contours. From Fig. 7.5, we also deduce that a significant amount of dimming is possible only for $g_{10}B_{\rm nG} \gtrsim 4 \times 10^{-2}$.

In CKT I, where the effect of n_e was neglected, $m_a \sim 10^{-16}\,\mathrm{eV}$ was used, corresponding to $n_{e,\rm eff} \approx 6 \times 10^{-12}\,\mathrm{cm}^{-3}$. As noted in CKT II, when plasma effects are taken into account, any value $n_e \lesssim 2.5 \times 10^{-8}\,\mathrm{cm}^{-3}$ guarantees the required achromaticity of the dimming below the 3% level between the B and V bands. The choice $B_{\rm nG}$ of a few and $g_{10} \approx 0.1$ in CKT I and II falls in the region where the observed SN-dimming could be explained while being marginally compatible with the bounds on the intergalactic B field and on the axion-photon coupling.

7.4 CMB Constraints

If photon-axion conversion over cosmological distances is responsible for the SN Ia dimming, the same phenomenon should also leave an imprint in the CMB. A similar argument was previously considered for photon-graviton conversion [31]. Qualitatively, in the energy-dependent region of $P_{\gamma\to a}$ one expects a rather small effect due to the low energy of CMB photons ($\omega \sim 10^{-4}\,\mathrm{eV}$). However, when accounting for the incoherent integration over many domains crossed by the photon, appreciable spectral distortions may arise in view of the accuracy of the CMB data at the level of one part in 10^4–10^5. For the same reason, in the energy-independent region, at much lower values of n_e than for the SNe Ia, the constraints on $g_{10}B_{\mathrm{nG}}$ are expected to be quite severe. The depletion of CMB photons in the patchy magnetic sky and its effect on the CMB anisotropy pattern have been previously considered [15]. However, more stringent limits come from the distortion of the overall blackbody spectrum [32].

To this end, the COBE/FIRAS data for the experimentally measured spectrum were used, corrected for foregrounds [33]. Note that the new calibration of FIRAS [34] is within the old errors and would not change any of our conclusions. The $N = 43$ data points Φ_i^{exp} at different energies ω_i are obtained by summing the best-fit blackbody spectrum (Fig. 7.6) to the residuals reported in [33]. The experimental errors σ_i and the correlation indices ϱ_{ij} between different energies are also available. In the presence of photon-axion conversion, the original intensity of the "theoretical blackbody" at temperature T

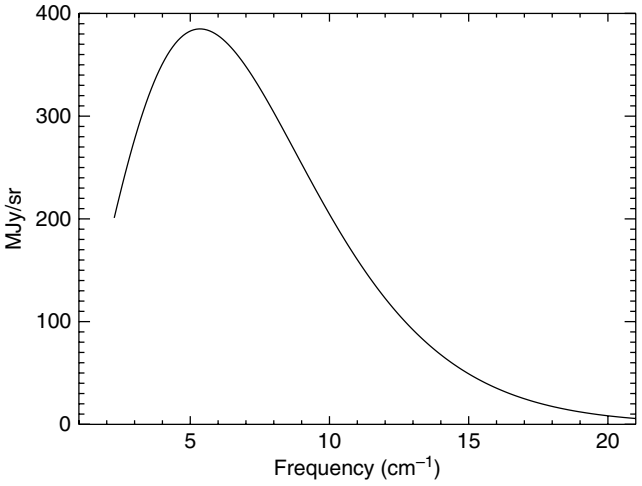

Fig. 7.6. Uniform CMB spectrum and fit to the blackbody spectrum. Uncertainties are a small fraction of the line thickness (Figure from [33] with permission)

$$\Phi^0(\omega, T) = \frac{\omega^3}{2\pi^2}\left[\exp(\omega/T) - 1\right]^{-1} \tag{7.26}$$

would convert to a deformed spectrum that is given by

$$\Phi(\omega, T) = \Phi^0(\omega, T) P_{\gamma\to\gamma}(\omega) \ . \tag{7.27}$$

In [32], we built the reduced chi-squared function

$$\chi^2_\nu(T, \lambda) = \frac{1}{N-1} \sum_{i,j=1}^{N} \Delta\Phi_i (\sigma^2)^{-1}_{ij} \Delta\Phi_j \ , \tag{7.28}$$

where

$$\Delta\Phi_i = \Phi_i^{\rm exp} - \Phi^0(\omega_i, T) P_{\gamma\to\gamma}(\omega_i, \lambda) \tag{7.29}$$

is the i-th residual, and

$$\sigma^2_{ij} = \varrho_{ij} \sigma_i \sigma_j \tag{7.30}$$

is the covariance matrix. We minimize this function with respect to T for each point in the parameter space $\lambda = (n_e, g_{10} B_{\rm nG})$; i.e., T is an empirical parameter determined by the χ^2_ν minimization for each λ rather than being fixed at the standard value $T_0 = 2.725 \pm 0.002$ K [34]. In principle, one should marginalize also over the galactic foreground spectrum [33]. However, this is a subleading effect relative to the spectral deformation caused by the photon-axion conversion.

In Fig. 7.7 we show the exclusion contour in the plane of n_e and $g_{10} B_{\rm nG}$. The region above the continuous curve is the excluded region at 95% CL, i.e., in this region the probability to get larger values of χ^2_ν is lower than 5%. We also show the corresponding 99% CL contour which is very close to the 95% contour so that another regression method and/or exclusion criterion would not change the results very much. Within a factor of a few, the same contours also hold if one varies the domain size s within a factor of 10. Comparing this exclusion plot with the iso-dimming curves of Fig. 7.5, we conclude that the entire region $n_e \lesssim 10^{-9}\,{\rm cm}^{-3}$ is excluded as a leading explanation for SN-dimming.

A few comments are in order. Intergalactic magnetic fields probably are a relatively recent phenomenon in the cosmic history, arising only at redshifts of a few. As a first approximation, we have considered the photon-axion conversion as happening for present ($z = 0$) CMB photons. As $P_{\gamma\to\gamma}$ is an increasing function of the photon energy ω, our approach leads to conservative limits. Moreover, we assumed no correlation between n_e and the intergalactic magnetic field strength. It is, however, physically expected that the fields are positively correlated with the plasma density so that relatively high values of $g_{10} B_{\rm nG}$ should be more likely when n_e is larger. Our constraints in the region of $n_e \gtrsim 10^{-10}\,{\rm cm}^{-3}$ are thus probably tighter than what naively appears.

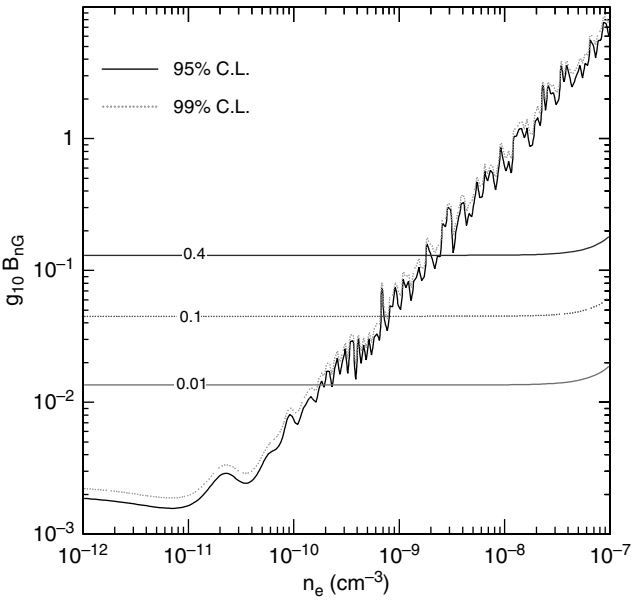

Fig. 7.7. Exclusion plot for axion-photon conversion based on the COBE/FIRAS CMB spectral data. The region above the solid curve is excluded at 95% CL whereas the one above the dotted curve is excluded at 99% CL. The size of each magnetic domain is fixed at $s = 1\,\mathrm{Mpc}$. We also reproduce the iso-dimming contours from Fig. 7.5 (Figure from [32] with permission)

7.5 QSO Constraints

CMB limits are nicely complementary to the ones obtained from the effects of photon-axion conversion on quasar colors and spectra [35]. One effect of photon-axion oscillations is that a dispersion is added to the quasar spectra due to the energy-dependence of the effect. By comparing the dispersion observed in quasar spectra with the dispersion in simulated ones, one can find out whether the model behind each simulation is allowed. The SuperNova Observation Calculator (SNOC) [36] was used [35] to simulate the effects of photon-axion oscillations on quasar observations (Fig. 7.8). If the simulated dispersion is smaller than observed, one cannot exclude the scenario as real quasars have an intrinsic dispersion.

In Fig. 7.9, we superimpose the CMB exclusion contours with the schematic region excluded by quasars[1]. The region to the right of the dot-dashed line is excluded by requiring achromaticity of SN Ia dimming [30]. The

[1] We use the exclusion regions of astro-ph/0410501v1. In the published version [35], corresponding to astro-ph/0410501v2, the iso-dimming curves were erroneously changed. The difference is that in version 1 the angle α in equation (3) of [35] that characterizes the random magnetic field direction was correctly taken in the

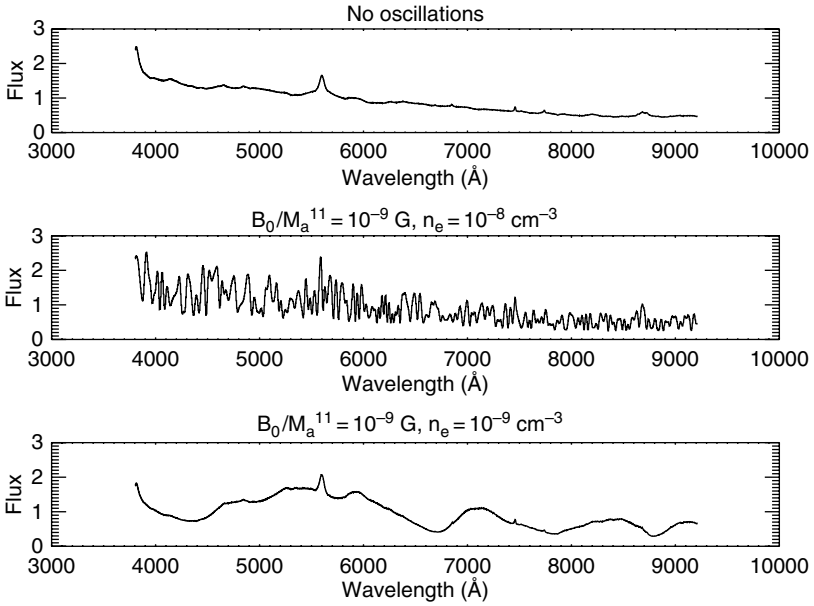

Fig. 7.8. Simulated quasar spectra at $z = 1$ for different photon-axion oscillation scenarios (Figure from [35] with permission)

region inside the dashed lines is excluded by the dispersion in QSO spectra. Moreover, assuming an intrinsic dispersion of 5% in these spectra, the excluded region could be enlarged up to the dotted lines. The CMB argument excludes the region above the solid curve at 95% CL.

A cautionary remark is in order when combining the two constraints. As we have discussed in the previous section, CMB limits on photon-axion conversion are model-independent. On the other hand, the limits placed by the QSO spectra may be subject to loop holes, as they are based on a full correlation between the intergalactic electron density and the magnetic field strength, which is reasonable but not well established observationally.

7.6 Constraints from Angular Diameter Distance

We now turn briefly to two other types of constraints on the photon-axion conversion mechanism. The first is based on angular diameter distance measurements of radio-galaxies. For a source of linear radius r and angular diameter θ, the angular diameter distance is

$$\mathrm{d}_A = \frac{2r}{\theta} \,. \tag{7.31}$$

interval 0–360°, whereas in version 2 it was taken in the interval 0–90° (private communication by the authors).

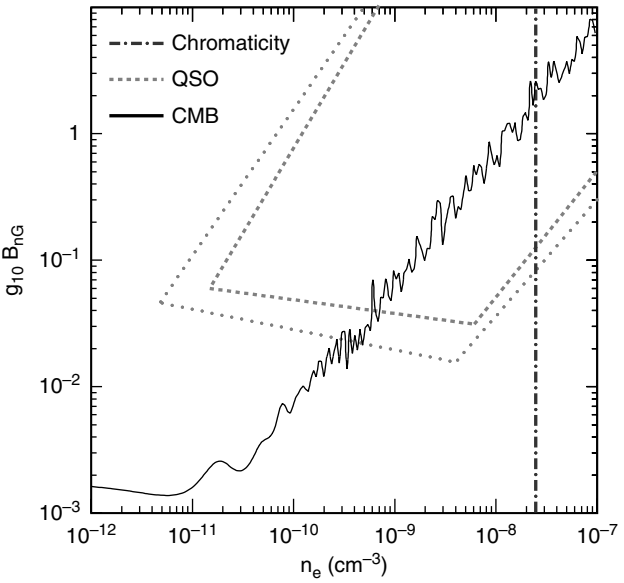

Fig. 7.9. Exclusion plot for photon-axion conversion. The region to the right of the dot-dashed line is excluded by requiring achromaticity of SN Ia dimming. The region inside the dashed lines is excluded by the dispersion in QSO spectra. Assuming an intrinsic dispersion of 5% in QSO spectra, the excluded region could be extended up to the dotted curve. The CMB argument excludes the entire region above the solid curve at 95% CL (Figure from [32] with permission)

In metric theories where photons travel on null geodesics and their number is conserved, the angular distance d_A and the luminosity distance d_L are fundamentally related by the reciprocity relation [37]

$$\mathrm{d}_L(z) = (1+z)^2 \mathrm{d}_A(z)\ . \tag{7.32}$$

Photon-axion conversion in intergalactic magnetic fields would not affect the angular-diameter distance [38, 39] and hence would cause a fundamental asymmetry between measurements of $\mathrm{d}_L(z)$ and $\mathrm{d}_A(z)$.

In a first search for a violation of the reciprocity relation, a joint analysis of high-redshift SNe Ia $[\mathrm{d}_L(z)]$ and radio galaxies $[\mathrm{d}_A(z)]$ was undertaken [38]. The results do not favor the loss of photons and hence disfavor mixing. However, this constraint is less robust than the QSO one because it is affected by possibly large systematic errors that are difficult to quantify [40].

As angular-diameter distance is immune to the loss of photons, the axion-conversion versus accelerating-universe ambiguity in the interpretation can be resolved [41] by combining CMB acoustic peak measurements with the recent detection of baryon oscillations in galaxy power spectra [42]. This

combination excludes a non-accelerating dark-energy species at the 4σ level regardless of the level of the axion coupling.

7.7 Conclusions

We have reviewed the intriguing and phenomenologically rich [43] mechanism of conversion of photons into very low-mass axion-like particles in the presence of intergalactic magnetic fields. We have examined the existing astrophysical and cosmological limits on this model, coming from the distortion of the CMB spectrum, from the quasar dispersion, and from the angular diameter distance, including the baryon oscillations detected in large-scale structure surveys.

In particular, we have shown that the resulting CMB spectral deformation excludes a previously allowed parameter region corresponding to very low densities of the intergalactic medium (IGM). These limits are complementary to the ones derived from QSO dispersion that place serious constraints on the axion-photon conversion mechanism, especially for relatively large densities of the IGM. As a result, it appears that the photon-axion conversion will not play a leading role for the apparent SN Ia dimming.

It may still happen that ultra-light or massless axions play an important cosmological role. For example, it was shown that by adding a photon-axion conversion mechanism on top of a dark-energy model with $w \gtrsim -1$, one can mimic cosmic equations of state as negative as $w \simeq -1.5$ [44]. Although at present there is no need for such an extreme equation of state, it is an interesting possibility to keep in mind, especially as alternative explanations as ghost/phantom fields usually pose a threat to very fundamental concepts in general relativity and quantum field theory.

Acknowledgments

A. Mirizzi and G. Raffelt thank the organizers of the Joint ILIAS-CAST-CERN Axion Training at CERN for their kind hospitality. In Munich, this work was supported, in part, by the Deutsche Forschungsgemeinschaft under grant No. SFB 375 and by the European Union under the ILIAS project, contract No. RII3-CT-2004-506222. A. Mirizzi was supported, in part, by the Istituto Nazionale di Fisica Nucleare (INFN) and by the Ministero dell'Istruzione, Università e Ricerca (MIUR) through the "Astroparticle Physics" research project.

Appendix A: A Photon-Axion Conversion in a Random Background

In the following, we derive (7.17) along the lines of [23]. It is assumed that photons and axions traverse N domains of equal length s. The component of the magnetic field perpendicular to the direction of flight $\mathbf{B}_{\rm T}$ is constant within each domain and of equal strength ($B \equiv |\mathbf{B}_{\rm T}|$) in each domain, but it is assumed to have a random orientation in each cell.

We begin with an initial state that is a coherent superposition of an axion and the two photon states $|A_{1,2}\rangle$ that correspond respectively to photons polarized parallel and perpendicular to the magnetic field in the first domain,

$$\kappa_1(0)|A_1\rangle + \kappa_2(0)|A_2\rangle + \kappa_a(0)|a\rangle \; . \tag{7.33}$$

The initial photon and axion fluxes are

$$I_\gamma(0) \sim |\kappa_1(0)|^2 + |\kappa_2(0)|^2 \; , \tag{7.34}$$

$$I_a(0) \sim |\kappa_a(0)|^2 \; , \tag{7.35}$$

respectively. In the n-th domain the transverse magnetic field $\mathbf{B}_{\rm T}$ is tilted by an angle γ_n compared to the magnetic field in the first domain

$$|A_\parallel^n\rangle = c_n|A_1\rangle + s_n|A_2\rangle \; , \tag{7.36}$$

$$|A_\perp^n\rangle = -s_n|A_1\rangle + c_n|A_2\rangle \; , \tag{7.37}$$

or

$$c_1(z) = c_n\kappa_\parallel^n(z) - s_n\kappa_\perp^n(z) \; , \tag{7.38}$$

$$c_2(z) = s_n\kappa_\parallel^n(z) + c_n\kappa_\perp^n(z) \; , \tag{7.39}$$

where $c_n = \cos\gamma_n$ and $s_n = \sin\gamma_n$. Only photons polarized parallel to the magnetic field mix with axions. The values of the transition elements are equal in each domain as the magnitude of the magnetic field B has been assumed to be the same everywhere. The transition probability P_0 for photon to axion oscillation in one domain is given by (7.15), and the photon survival probability is $1 - P_0$. At the end of the n-th domain, the photon and axion fluxes are

$$I_\gamma(n+1) \sim (1 - P_0c_n^2)|\kappa_1(z_n)|^2 \tag{7.40}$$

$$+(1 - P_0s_n^2)|\kappa_2(z_n)|^2 + P_0|\kappa_a(z_n)|^2 + \cdots \tag{7.41}$$

$$I_a(n+1) \sim P_0c_n^2|\kappa_1(z_n)|^2$$

$$+P_0s_n^2|\kappa_2(z_n)|^2 + (1 - P_0)|\kappa_a(z_n)|^2 + \cdots \tag{7.42}$$

where the dots represent terms that are proportional to c_n, s_n, or c_ns_n. We have defined $z_n = (n-1)s$. The coefficients κ_1, κ_2 and κ_a are taken at the beginning of the n-th domain.

Next, we assume that the transition probability in one domain is small, i.e., $P_0 \ll 1$, and the direction of the magnetic field is random, i.e., γ_n is a random variable so that $\gamma_{n+1} - \gamma_n$ is of order unity. Due to the randomness of the magnetic field, in this limit c_n^2 and s_n^2 can be replaced by their average value 1/2, while the interference terms c_n, s_n and $c_n s_n$ are averaged to zero. Using

$$I_\gamma(n) \sim |\kappa_1(z_n)|^2 + |\kappa_2(z_n)|^2 \,, \tag{7.43}$$

$$I_a \sim |\kappa_a(z_n)|^2 \,, \tag{7.44}$$

one arrives at

$$\begin{aligned} \begin{pmatrix} I_\gamma(n+1) \\ I_a(n+1) \end{pmatrix} &= \begin{pmatrix} 1 - \frac{1}{2}P_0 & P_0 \\ \frac{1}{2}P_0 & 1 - P_0 \end{pmatrix} \begin{pmatrix} I_\gamma(n) \\ I_a(n) \end{pmatrix} \\ &= \frac{1}{3} \begin{pmatrix} 2 + \left(1 - \frac{3}{2}P_0\right)^{n+1} & 2 - 2\left(1 - \frac{3}{2}P_0\right)^{n+1} \\ 1 - \left(1 - \frac{3}{2}P_0\right)^{n+1} & 1 + 2\left(1 - \frac{3}{2}P_0\right)^{n+1} \end{pmatrix} \begin{pmatrix} I_\gamma(0) \\ I_a(0) \end{pmatrix} . \end{aligned} \tag{7.45}$$

As the number of domains is large, one can replace $(1 - 3P_0/2)^{n+1}$ with the limiting function $\exp\left[-3P_0 z/(2s)\right]$ to arrive at the final expressions

$$I_\gamma(z) = I_\gamma(0) - P_{\gamma\to a}[I_\gamma(0) - 2I_a(0)] \,, \tag{7.46}$$

$$I_a(z) = I_a(0) + P_{\gamma\to a}[I_\gamma(0) - 2I_a(0)] \,, \tag{7.47}$$

with

$$P_{\gamma\to a} = \frac{1}{3}\left[1 - \exp\left(-\frac{3P_0 z}{2\,s}\right)\right] . \tag{7.48}$$

References

1. Sikivie, P.: Experimental tests of the 'invisible' axion. Phys. Rev. Lett. **51**, 1415 (1983), (E) ibid. **52**, 695 (1984)
2. Raffelt, G., Stodolsky, L.: Mixing of the photon with low mass particles. Phys. Rev. D **37**, 1237 (1988)
3. Bradley, R., et al.: Microwave cavity searches for dark-matter axions. Rev. Mod. Phys. **75**, 777 (2003)
4. van Bibber, K., McIntyre, P.M., Morris, D.E., Raffelt, G.G.: A practical laboratory detector for solar axions. Phys. Rev. D **39**, 2089 (1989)
5. Moriyama, S., Minowa, M., Namba, T., Inoue, Y., Takasu, Y., Yamamoto, A.: Direct search for solar axions by using strong magnetic field and X-ray detectors. Phys. Lett. B **434**, 147 (1998) [hep-ex/9805026]
6. Inoue, Y., Namba, T., Moriyama, S., Minowa, M., Takasu, Y., Horiuchi, T., Yamamoto, A.: Search for sub-electronvolt solar axions using coherent conversion of axions into photons in magnetic field and gas helium. Phys. Lett. B **536**, 18 (2002) [astro-ph/0204388]
7. Zioutas, K., et al. (CAST Collaboration): First results from the CERN axion solar telescope (CAST). Phys. Rev. Lett. **94**, 121301 (2005) [hep-ex/0411033]

8. Raffelt, G.G.: Stars as Laboratories for Fundamental Physics. University of Chicago Press, Chicago (1996)
9. Raffelt, G.G.: Particle physics from stars. Annu. Rev. Nucl. Part. Sci. **49**, 163 (1999) [hep-ph/9903472]
10. Harari, D., Sikivie, P.: Effects of a Nambu-Goldstone boson on the polarization of radio galaxies and the cosmic microwave background. Phys. Lett. B **289**, 67 (1992)
11. Hutsemekers, D., Cabanac, R., Lamy, H., Sluse, D.: Mapping extreme-scale alignments of quasar polarization vectors. Astron. Astrophys. **441**, 915 (2005) [astro-ph/0507274]
12. Krasnikov, S.V.: New astrophysical constraints on the light pseudoscalar photon coupling. Phys. Rev. Lett. **76**, 2633 (1996)
13. Gorbunov, D.S., Raffelt, G.G., Semikoz, D.V.: Axion-like particles as ultrahigh-energy cosmic rays?. Phys. Rev. D **64**, 096005 (2001) [hep-ph/0103175]
14. Csáki, C., Kaloper, N., Peloso, M., Terning, J.: Super-GZK photons from photon axion mixing. JCAP 0305, 005 (2003) [hep-ph/0302030]
15. Csáki, C., Kaloper, N., Terning, J.: (CKT I), Dimming supernovae without cosmic acceleration. Phys. Rev. Lett. **88**, 161302 (2002) [hep-ph/0111311]
16. Riess, A.G., et al. (Supernova Search Team Collaboration): Observational evidence from supernovae for an accelerating universe and a cosmological constant. Astron. J. **116**, 1009 (1998) [astro-ph/9805201]
17. Perlmutter, S., et al. (Supernova Cosmology Project Collaboration): Measurements of Ω and Λ from 42 high-redshift supernovae. Astrophys. J. **517**, 565 (1999) [astro-ph/9812133]
18. Riess, A.G., et al. (Supernova Search Team Collaboration): Type Ia supernova discoveries at $z > 1$ from the Hubble Space Telescope: Evidence for past deceleration and constraints on dark energy evolution. Astrophys. J. **607**, 665 (2004) [astro-ph/0402512]
19. Carroll, S.M.: Why is the universe accelerating? eConf C0307282 (2003) TTH09 [AIP Conf. Proc. **743**, 16 (2005), astro-ph/0310342]
20. Anselm, A.A.: Experimental test for arion $\leftrightarrow$ photon oscillations in a homogeneous constant magnetic field. Phys. Rev. D **37**, 2001 (1988)
21. Deffayet, C., Harari, D., Uzan, J.P., Zaldarriaga, M.: Dimming of supernovae by photon-pseudoscalar conversion and the intergalactic plasma. Phys. Rev. D **66**, 043517 (2002) [hep-ph/0112118]
22. Kuo, T.K., Pantaleone, J.T.: Neutrino oscillations in matter. Rev. Mod. Phys. **61**, 937 (1989)
23. Grossman, Y., Roy, S., Zupan, J.: Effects of initial axion production and photon axion oscillation on type Ia supernova dimming. Phys. Lett. B **543**, 23 (2002) [hep-ph/0204216]
24. Kronberg, P.P.: Extragalactic magnetic fields. Rept. Prog. Phys. **57**, 325 (1994)
25. Spergel, D.N., et al. (WMAP Collaboration): First year Wilkinson Microwave Anisotropy Probe (WMAP) observations: determination of cosmological parameters. Astrophys. J. Suppl. **148**, 175 (2003) [astro-ph/0302209]
26. Anselm, A.A., Uraltsev, N.G.: A second massless axion? Phys. Lett. B **114**, 39 (1982)
27. Anselm, A.A., Uraltsev, N.G.: Long range 'arion' field in the radiofrequency band. Phys. Lett. B **116**, 161 (1982)

28. Brockway, J.W., Carlson, E.D., Raffelt, G.G.: SN 1987A gamma-ray limits on the conversion of pseudoscalars. Phys. Lett. B **383**, 439 (1996) [astro-ph/9605197]
29. Grifols, J.A., Massó, E., Toldrà, R.: Gamma rays from SN 1987A due to pseudoscalar conversion. Phys. Rev. Lett. **77**, 2372 (1996) [astro-ph/9606028]
30. Csáki, C., Kaloper, N., Terning, J.: (CKT II), Effects of the intergalactic plasma on supernova dimming via photon axion oscillations. Phys. Lett. B **535**, 33 (2002) [hep-ph/0112212]
31. Chen, P.: Resonant photon-graviton conversion and cosmic microwave background fluctuations. Phys. Rev. Lett. **74**, 634 (1995); (E) ibid. **74**, 3091 (1995)
32. Mirizzi, A., Raffelt, G.G., Serpico, P.D.: Photon axion conversion as a mechanism for supernova dimming: Limits from CMB spectral distortion. Phys. Rev. D **72**, 023501 (2005) [astro-ph/0506078]
33. Fixsen, D.J., Cheng, E.S., Gales, J.M., Mather, J.C., Shafer, R.A., Wright, E.L.: The cosmic microwave background spectrum from the full COBE/FIRAS data set. Astrophys. J. **473**, 576 (1996) [astro-ph/9605054]
34. Mather, J.C., Fixsen, D.J., Shafer, R.A., Mosier, C., Wilkinson, D.T.: Calibrator design for the COBE far infrared absolute spectrophotometer (FIRAS). Astrophys. J. 512 (1999) 511 [astro-ph/9810373]
35. Ostman, L., Mörtsell, E.: Limiting the dimming of distant type Ia supernovae. JCAP 0502, 005 (2005) [astro-ph/0410501]
36. Goobar, A., Mörtsell, E., Amanullah, R., Goliath, M., Bergström, L., Dahlen, T.: SNOC: a Monte-Carlo simulation package for high-z supernova observations. Astron. Astrophys. **392**, 757 (2002) [astro-ph/0206409]
37. Schneider, P., Ehlers, J., Falco, E.E.: Gravitational lenses. Springer-Verlag, Berlin (1992)
38. Bassett, B.A., Kunz, M.: Cosmic acceleration versus axion photon mixing. Astrophys. J. **607**, 661 (2004) [astro-ph/0311495]
39. Bassett, B.A., Kunz, M.: Cosmic distance-duality as a probe of exotic physics and acceleration. Phys. Rev. D **69**, 101305 (2004) [astro-ph/0312443]
40. Uzan, J.P., Aghanim, N., Mellier, Y.: The distance duality relation from X-ray and Sunyaev-Zel'dovich observations of clusters. Phys. Rev. D **70**, 083533 (2004) [astro-ph/0405620]
41. Song, Y.S., Hu, W.: Constraints on supernovae dimming from photon-pseudo scalar coupling. Phys. Rev. D **73**, 023003 (2006) [astro-ph/0508002]
42. Eisenstein, D.J., et al.: Detection of the baryon acoustic peak in the large-scale correlation function of SDSS luminous red galaxies. Astrophys. J. **633**, 560 (2005) [astro-ph/0501171]
43. Das, S., Jain, P., Ralston, J.P., Saha, R.: Probing dark energy with light: Propagation and spontaneous polarization. JCAP 0506, 002 (2005) [hep-ph/0408198]
44. Csáki, C., Kaloper, N., Terning, J.: Exorcising $w < -1$. Annals Phys. **317**, 410 (2005) [astro-ph/0409596]